PHYSICS

Anti–parity-time symmetry in diffusive systems

Ying Li[1]*, Yu-Gui Peng[1,2]*, Lei Han[1,3]*, Mohammad-Ali Miri[4,5], Wei Li[6], Meng Xiao[6,7], Xue-Feng Zhu[2]†, Jianlin Zhao[3], Andrea Alù[4,8,9,10], Shanhui Fan[6]†, Cheng-Wei Qiu[1]†

Various concepts related to parity-time symmetry, including anti–parity-time symmetry, have found broad applications in wave physics. Wave systems are fundamentally described by Hermitian operators, whereas their unusual properties are introduced by incorporation of gain and loss. We propose that the related physics need not be restricted to wave dynamics, and we consider systems described by diffusive dynamics. We study the heat transfer in two countermoving media and show that this system exhibits anti–parity-time symmetry. The spontaneous symmetry breaking results in a phase transition from motionless temperature profiles, despite the mechanical motion of the background, to moving temperature profiles. Our results extend the concepts of parity-time symmetry beyond wave physics and may offer opportunities to manipulate heat and mass transport.

Quantum physics has shown that a non-Hermitian Hamiltonian operator can exhibit entirely real spectra (*1*, *2*) when parity-time (PT) symmetry is preserved. The studies on this concept are especially fruitful in classical wave systems (*3*–*7*), where PT symmetry is manifested as balanced gain and loss. Spontaneous symmetry breaking happens when the system is tuned across an exceptional point (EP) (*8*–*11*), and this is related to many intriguing phenomena (*12*–*19*). Recently, anti-PT (APT) symmetric systems also have been of interest (*20*–*25*). The Hamiltonian H of such a system is mapped to its opposite by parity ($\mathcal{P}$) and time-reversal ($\mathcal{T}$) operators. Such systems are known to exhibit noteworthy effects, such as energy difference–conserving dynamics (*23*), coherent switch (*24*), and constant refraction (*25*).

Earlier work on PT and/or APT symmetry was carried out in wave systems whose underlying physics is described by a Hermitian operator. Non-hermiticity then emerges by introducing gain or loss [dissipation with a negative or positive decay rate (blue dots in Fig. 1A)]. Because non-Hermitian physics is closely related to dissipation, one should be able to explore it in processes that are intrinsically dissipative as well, such as heat or mass transfer described by the diffusion equation. To date, studies of PT-related physics in diffusion are lacking. Here, we introduce a route to explore APT symmetry in heat transfer. Starting from purely dissipative heat conduction, we then introduce oscillatory (Hermitian) components to achieve the required symmetry (red dots in Fig. 1A). This idea motivates us to use heat convection (*26*) in moving media. Mechanical motion generally "drags" waves (*27*, *28*) or heat (*29*, *30*). Notably, we found that for heat convection, the temperature profile can stay still ($v_{\mathrm{Temp}} = 0$) despite the flow ($v > 0$) in the APT symmetric phase. In the symmetry-broken phase, the temperature profile can either follow the flow ($v_{\mathrm{Temp}} > 0$) or even move against it ($v_{\mathrm{Temp}} < 0$). Therefore, all three scenarios in Fig. 1B are possible.

We consider heat convection in two channels with opposite background velocities that are coupled by heat conduction (Fig. 1C) [three-dimensional (3D) version in Fig. 1D]. We denote the temperature field in the upper (or lower) channel with velocity v (or $-v$) as T_1 (or T_2). Consider a simple model of these temperature fields (*26*)

$$\frac{\partial T_1}{\partial t} = D\frac{\partial^2 T_1}{\partial x^2} - v\frac{\partial T_1}{\partial x} + h(T_2 - T_1)$$
$$\frac{\partial T_2}{\partial t} = D\frac{\partial^2 T_2}{\partial x^2} + v\frac{\partial T_2}{\partial x} + h(T_1 - T_2) \quad (1)$$

where D is the diffusivity, h is the rate of heat exchange between the two channels, t is the time, and x is the position. Using plane-wave solutions, Eq. 1 is reduced to an eigenvalue problem for the

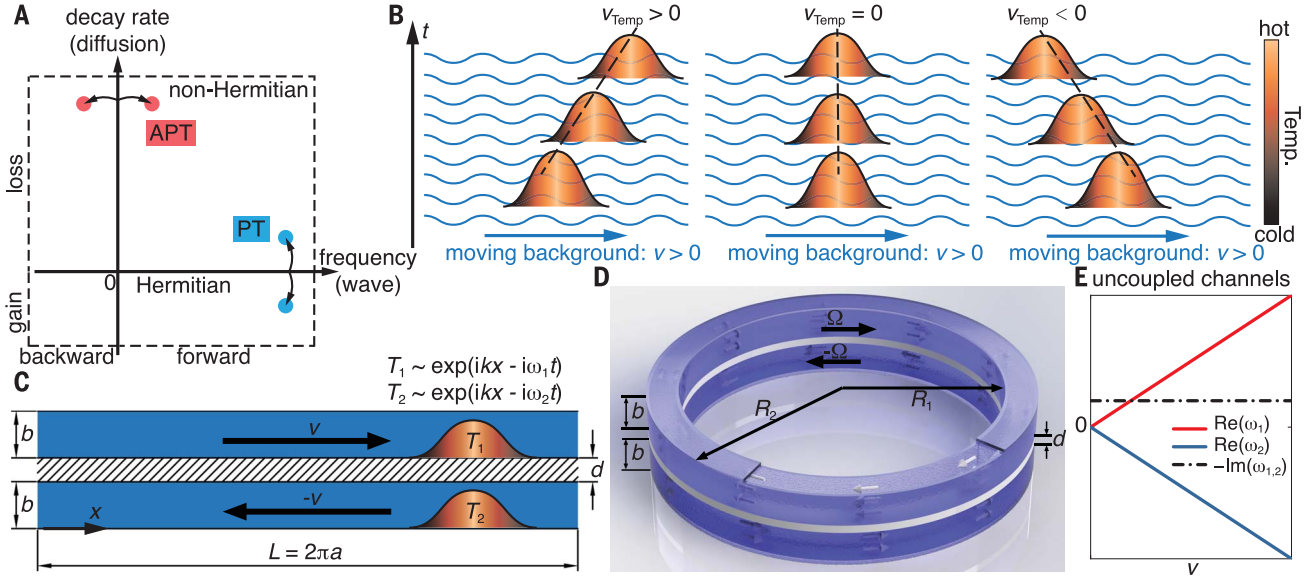

Fig. 1. APT symmetric diffusive system. (**A**) Two routes to explore non-Hermitian physics: from a wave system with zero decay rate (the abscissa) or from a diffusive system with zero frequency (the ordinate). (**B**) For heat convection, the temperature profile can follow, remain motionless, or move against the moving background. (**C**) A 2D model of an APT symmetric system. *b*, channel width; *d*, thickness. (**D**) A 3D model. R_1, interior ring radius; R_2, exterior ring radius. (**E**) The eigenfrequency of heat convection in the uncoupled limit. Re, real; Im, imaginary.

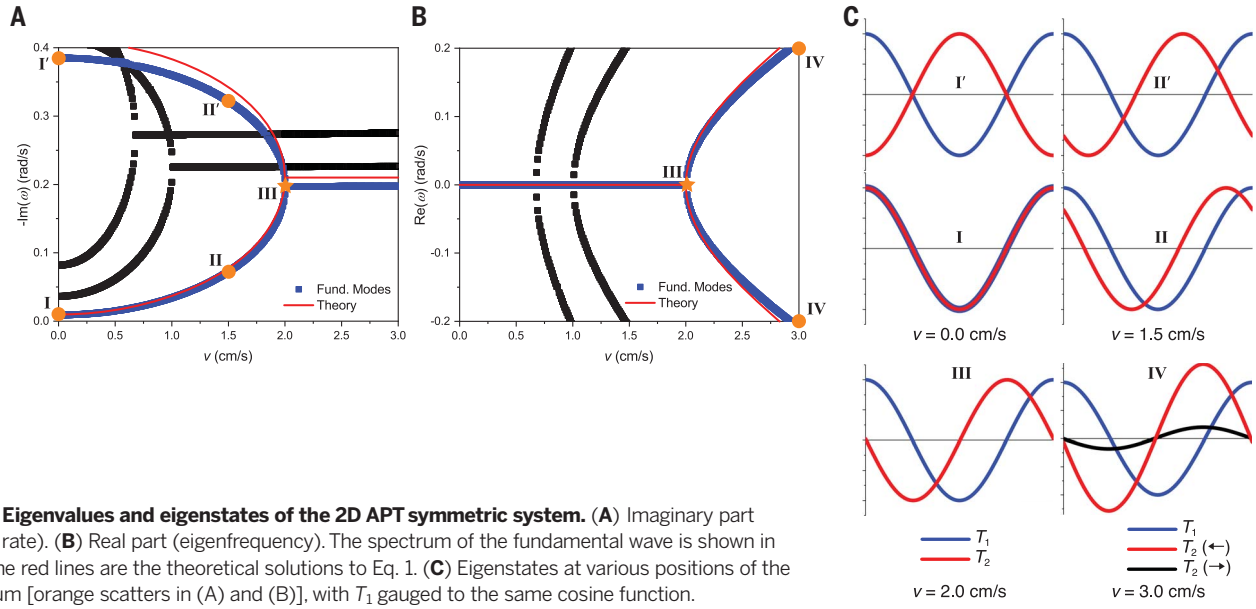

Fig. 2. Eigenvalues and eigenstates of the 2D APT symmetric system. (**A**) Imaginary part (decay rate). (**B**) Real part (eigenfrequency). The spectrum of the fundamental wave is shown in blue. The red lines are the theoretical solutions to Eq. 1. (**C**) Eigenstates at various positions of the spectrum [orange scatters in (A) and (B)], with T_1 gauged to the same cosine function.

effective Hamiltonian H, which is APT symmetric (materials and methods S1),

$$H = \begin{pmatrix} -i(k^2D+h)+kv & ih \\ ih & -i(k^2D+h)-kv \end{pmatrix} \quad (2)$$

where k is the wave number. The eigenvalue can be solved as

$$\omega_{\pm} = -i\left[(k^2D+h) \pm \sqrt{h^2-k^2v^2}\right] \quad (3)$$

In the uncoupled limit with $h = 0$, the system exhibits only a single phase, in which the eigenvalues always have a nonzero real part at $v \neq 0$ (Fig. 1E). When $h \neq 0$, this system exhibits two phases as v varies. For small v, the system is in the symmetric phase with purely imaginary eigenvalues. The corresponding eigenstates preserve APT symmetry. With large v, the system is in the symmetry-broken phase, where the eigenvalues have nonzero real parts (materials and methods S1). The transition between the two phases occurs at the EP, $k^2v_{EP}^2 = h^2$, where v_{EP} is the critical velocity, which depends on k (supplementary text S1 and figs. S1 and S2).

We study the eigenvalue ω of the system in Fig. 1C with finite element simulations (materials and methods S2). Periodic boundary conditions are applied on the channels with length L, which only allows for discrete wave number $k = n/a$ (where n is an integer and $a = L/2\pi$). As v increases, the two branches of –Im(ω) coalesce at the EP, and then nonzero Re(ω) appears, as well described by the analytical model in Eq. 3

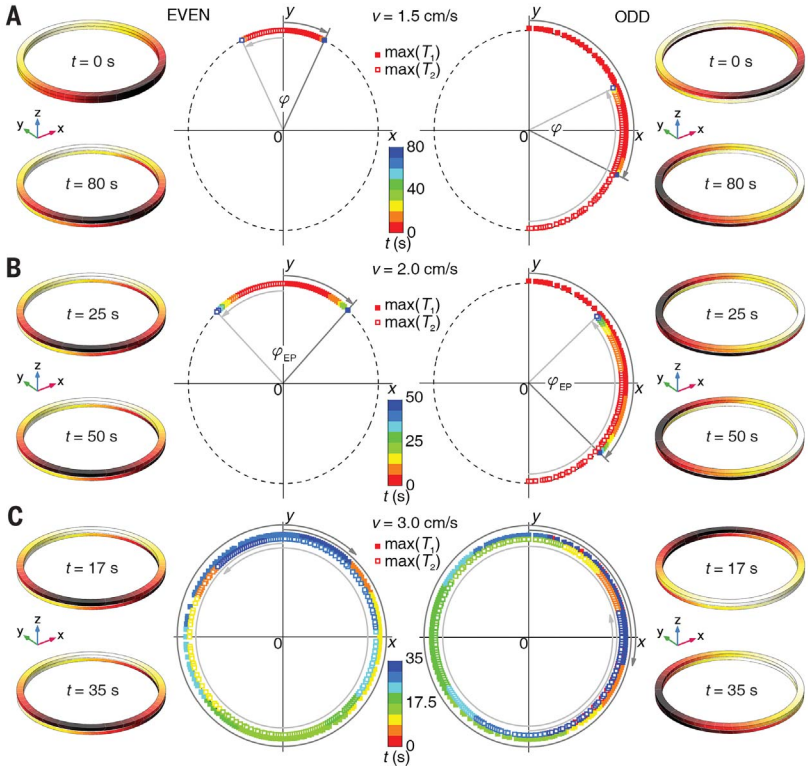

Fig. 3. Transient evolution of temperature profiles in the 3D APT symmetric system. Profiles for three velocities v are shown: 1.5 cm/s (**A**), 2.0 cm/s (**B**), and 3.0 cm/s (**C**). Snapshots of the temperature profiles are shown at the left and right sides, where the bright (dark) color represents hot (cold). In the center, we plot the trajectories of max(T_1) and max(T_2) along the interior edges of the rings (dashed circles), with scatters colored according to the time.

[1]Department of Electrical and Computer Engineering, National University of Singapore, Singapore 117583, Singapore. [2]School of Physics and Innovation Institute, Huazhong University of Science and Technology, Wuhan 430074, China. [3]MOE Key Laboratory of Material Physics and Chemistry under Extraordinary Conditions and Shaanxi Key Laboratory of Optical Information Technology, School of Natural and Applied Sciences, Northwestern Polytechnical University, Xi'an 710072, China. [4]Department of Electrical and Computer Engineering, The University of Texas at Austin, Austin, TX 78712, USA. [5]Department of Physics, Queens College, City University of New York, Queens, NY 11367, USA. [6]Department of Electrical Engineering, Ginzton Laboratory, Stanford University, Stanford, CA 94305, USA. [7]School of Physics and Technology, Wuhan University, Wuhan 430072, China. [8]Photonics Initiative, Advanced Science Research Center, City University of New York, New York, NY 10031, USA. [9]Physics Program, Graduate Center, City University of New York, New York, NY 10026, USA. [10]Department of Electrical Engineering, City College of New York, New York, NY 10031, USA.
*These authors contributed equally to this work.
†Corresponding author. Email: xfzhu@hust.edu.cn (X.-F.Z.); shanhui@stanford.edu (S.F.); chengwei.qiu@nus.edu.sg (C.-W.Q.)

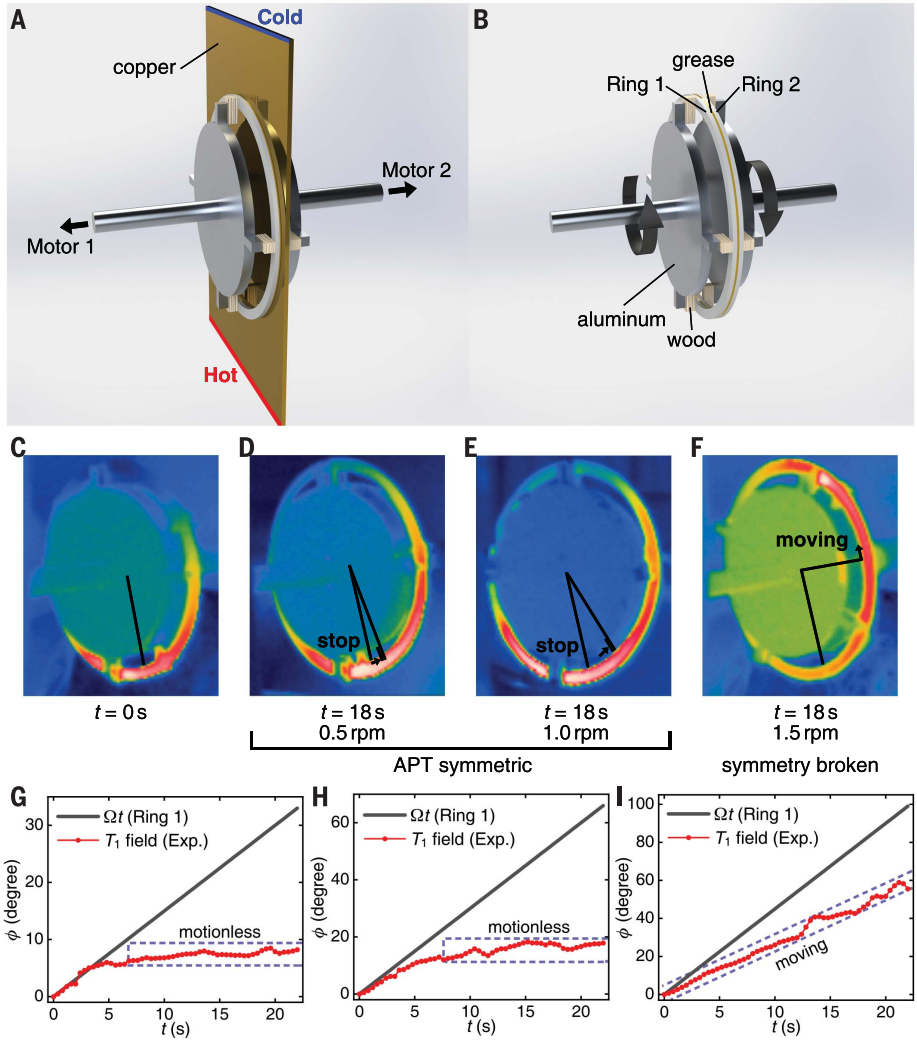

Fig. 4. Experimental setup and results for the APT symmetric and symmetry-broken phases. (**A** and **B**) Schematic graphs of the experimental setup for generating the initial temperature gradient (A) and performing transient measurements (B). (**C** to **F**) Infrared images of the temperature profiles on ring 1. (C) Snapshot taken at t = 0 s when the motors were just turned on. (D to F) Snapshots taken at t = 18 s for rings rotating at 0.5 rpm (D), 1.0 rpm (E), and 1.5 rpm (F). The colors from dark blue to red represent low to high temperatures, respectively. (**G** to **I**) Evolution of the temperature field T_1, represented as the rotation angle ϕ of the temperature dipole from the initial state, with a rotation speed Ω of 0.5 rpm (G), 1.0 rpm (H), and 1.5 rpm (I). The dark gray lines represent the rotation angles of ring 1.

(Fig. 2, A and B). Next, we focus on the fundamental modes with $\pm k_0 = \pm a^{-1}$ and track the eigenstates by looking at the temperature profiles along the upper and lower boundaries of the system, representing T_1 and T_2, respectively. The changes of profiles exactly follow the theoretical prediction (Fig. 2C). At v = 0 cm/s, the two eigenstates have even and odd symmetries with respect to the mirror plane between the channels. As v increases, T_2 gradually accumulates a negative (positive) phase along the lower (upper) branch of eigenvalues. At v_{EP} = 2 cm/s, the two profiles of T_2 coincide with one another, with $\pi/2$ phase behind T_1. For $v > v_{EP}$, the profiles start moving, because the system acquires nonzero eigenfrequency. At v = 3.0 cm/s, the amplitude of the forward wave ($+x$) is 0.38, whereas that of the backward wave ($-x$) is 1/0.38 = 2.61. These values agree well with the theoretical requirement.

The phase transition of temperature profiles across the EP can also be observed directly in the transient behavior. To do so, we numerically simulate a 3D system of two ring-shaped channels packed vertically (Fig. 1D). We define T_1 and T_2 as the temperatures along the upper and lower interior edges of the rings (interior radius $R_1 = a$). To induce the fundamental modes, we set the initial states as the eigenstates at v = 0 cm/s, namely, the same (even) or opposite (odd) temperature gradients along y in the two rings (materials and methods S3). With the same wave number $\pm k_0$, the initial states are expected to evolve to the fundamental modes for nonzero v.

One way to follow the evolution of the profiles of T_1 and T_2 is to follow their maximum points. The trajectories of max(T_1) and max(T_2) are shown with snapshots of the temperature profiles in the left and right panels of Fig. 3, A to C. At low speeds, the maximum points move from their initial positions to certain positions and stops (Fig. 3A). The temperature profile remains motionless thereafter for both initial conditions. For the even initial condition, the temperature profile directly evolves into the eigenstate illustrated in II of Fig. 2C, with T_1 ahead of T_2 for a phase ϕ that is less than $\pi/2$. For the odd initial condition, the temperature profile also eventually evolves into the same state as for the even initial condition. This is due to the typical nonorthogonality of the two eigenstates at different branches (*2*), so an odd initial condition also can evolve to the eigenstate at the lower branch of Fig. 2A, which decays much slower than the other eigenstate and eventually becomes the observed one.

At the EP when v = 2.0 cm/s, the motions are almost the same as when v is lower. Only the accumulated phase difference ϕ_{EP} is larger (Fig. 3B). This phase is found numerically to be $\phi_{EP} = 0.48\pi$, close to the analytically predicted $\pi/2$. At $v > 2.0$ cm/s, the temperature profiles are always in motion (scatters in Fig. 3C). The profile in each channel follows the background velocity direction, due to the broken APT symmetry of the state with complex eigenvalue.

The finite eigenfrequency indicates a moving temperature profile, but its direction does not necessarily have to follow that of the background. In fact, details of the symmetry-broken states depend on the initial condition. Numerical simulations reveal that the symmetry-broken phase can exhibit temperature flow opposite to the background motion, when an asymmetric initial condition is used (supplementary text S2 and fig. S3).

To observe the phenomena predicted in Fig. 3, we propose the experimental setup in Fig. 4, A and B (see also materials and methods S4 and fig. S4). The system consists of two plastic rings rotated by motors. The two solid rings exchange heat through a layer of lubricating grease. The heat exchange rate h of the grease layer can be estimated as 0.13 s^{-1}, which gives a critical rotation speed of ≈1.27 rpm. We first vertically place a copper plate, whose bottom (top) end is in a hot (cold) bath. The two rings are then brought in contact with the copper plate to achieve the vertical temperature gradient (Fig. 4A). After reaching steady state, we quickly remove the copper plate, make the two rings contact, and turn on the two motors so that the rings rotate in opposite directions with the same rotation speed Ω (Fig. 4B). An infrared camera is used to observe and record the evolution of the temperature field during the whole process (movies S1 to S3).

A snapshot of the temperature profiles on ring 1 at 0 s (when the motors were turned on) is shown in Fig. 4C, and snapshots at 18 s are shown in Fig. 4, D to F. At slower rotation speeds (0.5 and 1.0 rpm), the high-temperature regions are fixed after a small rotation from the initial place (Fig. 4, D and E), demonstrating the symmetric phase. On the contrary, at a faster rotation speed of 1.5 rpm, the high-temperature region is continuously moving (Fig. 4F), demonstrating the symmetry-broken phase. To further calibrate this rotation of temperature field, we postprocess the infrared images to calculate a "temperature dipole" $\mathbf{p}_T$ (materials and methods S4). The angle $\phi(t)$ between $\mathbf{p}_T(t)$ and $\mathbf{p}_T(0)$ is plotted in Fig. 4, G to I. Its rotation again confirms the phase transition.

This work reveals that APT symmetry can be realized with common materials in diffusion, which is outside wave physics. What establishes the symmetry is the opposite velocities of the two channels; this is different from previous systems that require opposite signs in material parameters (*3*–*6*) or require rescaling (*10*, *16*). Our findings open opportunities for using diffusive dynamics to study PT-related physics and provide insight into the development of control mechanisms in the broad area of nonequilibrium mass or energy transport.

REFERENCES AND NOTES

1. C. M. Bender, S. Boettcher, *Phys. Rev. Lett.* **80**, 5243–5246 (1998).
2. C. M. Bender, *Rep. Prog. Phys.* **70**, 947–1018 (2007).
3. K. G. Makris, R. El-Ganainy, D. N. Christodoulides, Z. H. Musslimani, *Phys. Rev. Lett.* **100**, 103904 (2008).
4. C. E. Rüter *et al.*, *Nat. Phys.* **6**, 192–195 (2010).
5. B. Peng *et al.*, *Nat. Phys.* **10**, 394–398 (2014).
6. X. Zhu, H. Ramezani, C. Shi, J. Zhu, X. Zhang, *Phys. Rev. X* **4**, 031042 (2014).
7. R. El-Ganainy *et al.*, *Nat. Phys.* **14**, 11–19 (2018).
8. W. D. Heiss, *J. Phys. Math. Gen.* **45**, 444016 (2012).
9. B. Peng *et al.*, *Science* **346**, 328–332 (2014).
10. A. Guo *et al.*, *Phys. Rev. Lett.* **103**, 093902 (2009).
11. L. Chang *et al.*, *Nat. Photonics* **8**, 524–529 (2014).
12. Z. Lin *et al.*, *Phys. Rev. Lett.* **106**, 213901 (2011).
13. A. Regensburger *et al.*, *Nature* **488**, 167–171 (2012).
14. L. Feng *et al.*, *Nat. Mater.* **12**, 108–113 (2013).
15. Z. J. Wong *et al.*, *Nat. Photonics* **10**, 796–801 (2016).
16. L. Feng, Z. J. Wong, R.-M. Ma, Y. Wang, X. Zhang, *Science* **346**, 972–975 (2014).
17. H. Hodaei, M.-A. Miri, M. Heinrich, D. N. Christodoulides, M. Khajavikhan, *Science* **346**, 975–978 (2014).
18. S. Assawaworrarit, X. Yu, S. Fan, *Nature* **546**, 387–390 (2017).
19. M.-A. Miri, A. Alù, *Science* **363**, eaar7709 (2019).
20. J.-H. Wu, M. Artoni, G. C. La Rocca, *Phys. Rev. Lett.* **113**, 123004 (2014).
21. J.-H. Wu, M. Artoni, G. C. La Rocca, *Phys. Rev. A* **91**, 033811 (2015).
22. P. Peng *et al.*, *Nat. Phys.* **12**, 1139–1145 (2016).
23. Y. Choi, C. Hahn, J. W. Yoon, S. H. Song, *Nat. Commun.* **9**, 2182 (2018).
24. V. V. Konotop, D. A. Zezyulin, *Phys. Rev. Lett.* **120**, 123902 (2018).
25. F. Yang, Y.-C. Liu, L. You, *Phys. Rev. A* **96**, 053845 (2017).
26. A. Bejan, *Convection Heat Transfer* (Wiley, 2013).
27. S. Franke-Arnold, G. Gibson, R. W. Boyd, M. J. Padgett, *Science* **333**, 65–67 (2011).
28. R. Fleury, D. L. Sounas, C. F. Sieck, M. R. Haberman, A. Alù, *Science* **343**, 516–519 (2014).
29. D. Torrent, O. Poncelet, J.-C. Batsale, *Phys. Rev. Lett.* **120**, 125501 (2018).
30. Y. Li *et al.*, *Nat. Mater.* **18**, 48–54 (2019).

ACKNOWLEDGMENTS

Funding: C.-W.Q. acknowledges financial support from the Ministry of Education, Singapore (project R-263-000-C05-112). X.-F.Z. and Y.-G.P. acknowledge the financial support of the National Natural Science Foundation of China (grants 11674119, 11690030, and 11690032) and the Bird Nest Plan of HUST. W.L. and S.F. acknowledge the support of U.S. Department of Energy grant DE-FG-07ER46426. **Author contributions:** Y.L. and C.-W.Q. conceived the concept. Y.L., S.F., and C.-W.Q. designed the model. Y.L. performed the numerical simulations. Y.L., M.-A.M., W.L., J.Z., A.A., and C.-W.Q. discussed the theoretical results and analyzed the model. Y.L., Y.-G.P., and L.H. prepared the samples and performed the experiments. X.-F.Z., S.F., and C.-W.Q. supervised the research. All authors discussed and contributed to the manuscript. **Competing interests:** The authors declare no competing interests. **Data and materials availability:** All data are available in the main text or the supplementary materials.

SUPPLEMENTARY MATERIALS

www.sciencemag.org/content/364/6436/170/suppl/DC1
Materials and Methods
Supplementary Text
Figs. S1 to S4
References (*31*–*40*)
Movies S1 to S3

10 January 2019; accepted 14 March 2019
10.1126/science.aaw6259

Anti–parity-time symmetry in diffusive systems

Ying Li, Yu-Gui Peng, Lei Han, Mohammad-Ali Miri, Wei Li, Meng Xiao, Xue-Feng Zhu, Jianlin Zhao, Andrea Alù, Shanhui Fan and Cheng-Wei Qiu

Science **364** (6436), 170-173.
DOI: 10.1126/science.aaw6259

Making heat stand still

Dissipative oscillating systems (waves) can be described mathematically in terms of non-Hermitian physics. When parity-time symmetric systems have dissipative components, the interplay between gain and loss can lead to unusual and exotic behavior. Li *et al.* show theoretically and demonstrate experimentally that such behavior need not be limited to wave systems. Looking at the diffusion of heat, they devised an experimental setup comprising two thermally coupled disks rotating in opposite directions. The thermal energy transported by each disk is strongly coupled to the disk rotating in the opposite direction, providing a return path for the heat wave. For a particular rotation rate, there is an exceptional point where thermal coupling and counterrotating motion balance, resulting in the thermal energy profile being stationary over time.

Science, this issue p. 170